# The Crystal Structures of Four Peptide Deformylases Bound to the Antibiotic Actinonin Reveal Two Distinct Types: A Platform for the Structure-based Design of Antibacterial Agents

**ARTICLE** *in* JOURNAL OF MOLECULAR BIOLOGY · AUGUST 2002

Impact Factor: 4.33 · DOI: 10.1016/S0022-2836(02)00549-1 · Source: PubMed

doi:10.1016/S0022-2836(02)00549-1 available online at http://www.idealibrary.com on IDEAL® J. Mol. Biol. (2002) 320, 951–962

JMB

# The Crystal Structures of Four Peptide Deformylases Bound to the Antibiotic Actinonin Reveal Two Distinct Types: A Platform for the Structure-based Design of Antibacterial Agents

**Jean-Pierre Guilloteau[1], Magali Mathieu[1], Carmela Giglione[2], Véronique Blanc[1], Alain Dupuy[1], Miline Chevrier[1], Patricia Gil[1], Alain Famechon[1], Thierry Meinnel[2] and Vincent Mikol[1]***

[1]*Drug Innovation & Approval Aventis Pharma, 13 Quai Jules Guesde, BP.14, F-94403 Vitry-sur-Seine, France*

[2]*Protein Maturation Trafficking and Signalling Institut des Sciences du Végétal UPR2355, Centre National de la Recherche Scientifique, 1 avenue de la Terrasse, F-91198 Gif-sur-Yvette Cedex, France*

**Corresponding author*

Bacterial peptide deformylase (PDF) belongs to a sub-family of metalloproteases that catalyse the removal of the N-terminal formyl group from newly synthesised proteins. PDF is essential in prokaryotes and conserved throughout the eubacteria. It is therefore considered an attractive target for developing new antibacterial agents. Here, we report the crystal structures of four bacterial deformylases, free or bound to the naturally occurring antibiotic actinonin, including two from the major bacterial pathogens *Pseudomonas aeruginosa* and *Staphylococcus aureus*. The overall tertiary structure is essentially conserved but shows significant differences, namely at the C terminus, which are directly related to the deformylase type (i.e. I or II) they belong to. The geometry around the catalytic metal ion exhibits a high level of similarity within the different enzymes, as does the binding mode of actinonin to the various deformylases. However, some significant structural differences are found in the vicinity of the active site, highlighting the structural and molecular requirements for the design of a deformylase inhibitor active against a broad spectrum of bacterial strains.



*Keywords:* actinonin; antibiotic; metalloprotease; crystal structure; inhibitor

## Introduction

In prokaryotes, protein synthesis begins with a formylated methionine residue.[1] Following translation initiation, the formyl group at the N terminus of the growing polypeptide is removed by peptide deformylase (PDF, EC 3.5.1.88).[2–4] Although N-formylation is not strictly essential for the survival of all bacterial species, it can stimulate protein synthesis by facilitating the use of Met-tRNA$^{fMet}$ in translation initiation and by preventing its recognition by the elongation apparatus.[5] Deformylation of peptides after translation is apparently a unique feature of bacterial cells and was shown to be essential in *Escherichia coli*, *Streptococcus pneumoniae* and *Staphylococcus aureus*.[6–9] The gene encoding PDF (*def*) is thought to be present in all sequenced bacterial genomes. Recently, gene sequences similar to *def* have been identified in the nucleus of most higher eukaryotes. Although the corresponding proteins were shown to be exported in plant organelles, neither their function nor their location have been established in mammals.[10,11] Nevertheless this has qualified PDF as an attractive target for the development of new antibacterial drugs.[12–14]

PDF was first isolated as an almost inactive but thermodynamically stable zinc complex[15] but it was shown later that the native enzyme is highly active and very likely utilizes Fe(II) as the catalytic metal ion.[16,17] Interestingly the ferrous ion can be replaced with a nickel or cobalt ion, resulting in no or little loss of activity but significantly enhanced stability.[16,18,19] Actinonin, a naturally occurring hydroxamic acid pseudopeptide was discovered 40 years ago[20] and was tested extensively for antibacterial activity in the 1970s.[21,22] It

Abbreviations used: PDF, peptide deformylase; r.m.s.d., root-mean-square deviation.

E-mail address of the corresponding author: vincent.mikol@aventis.com

 

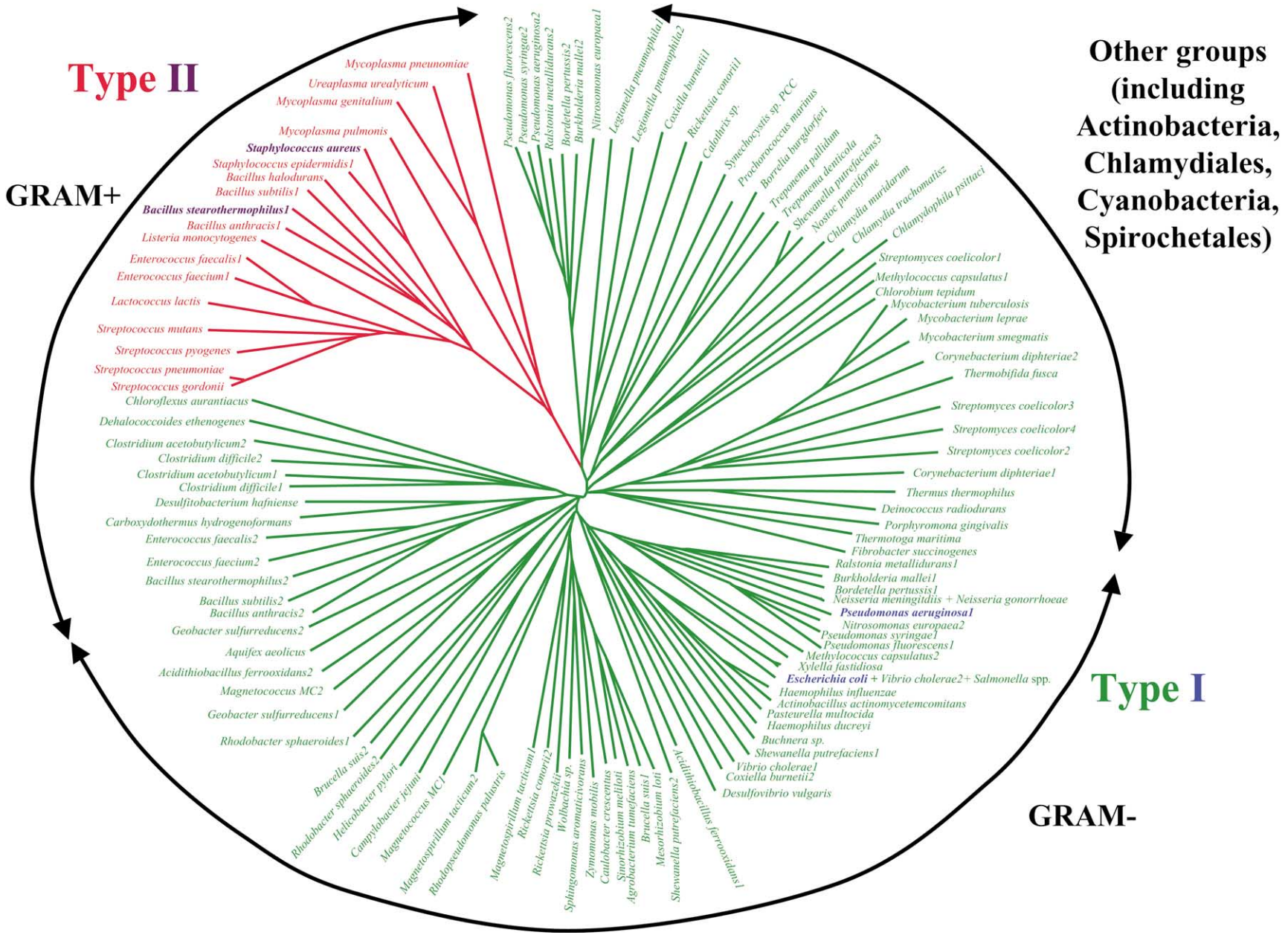


**Figure 1** (*legend opposite*)

was shown later that actinonin is a potent PDF inhibitor with a binding constant lying in the nanomolar range that exhibits bacteriostatic activity against Gram-positive microorganisms.[12,23] Recently, crystal structures and the solution structure of *E. coli* PDF have been determined, as was the crystal structure of actinonin in complex with *E. coli* PDF. Together with mutagenesis data,[24–28] this identified PDF as a new class of metalloenzyme related in structure to the metalloproteinase superfamily.[12] Recently, the structure of *Plasmodium falciparum* has been determined. It displays a very strong resemblance to the *E. coli* PDF.[29] The *E. coli* PDF was described as an α/β type protein where a central helix (αI) is wrapped by a five-stranded anti-parallel β-sheet and by a two-stranded anti-parallel β-sheet. Two helices, αA at the N terminus and αJ at the C terminus, lie on the outer surface. Both histidine residues from the conserved zinc hydrolase sequence HExxH motif that coordinate the catalytic metal atom are located in the central helix (αI), whereas the third ligand, a conserved cysteine residue lies at the end of strand βE and a water molecule serves as the fourth ligand.[26,30,31]

In this study, we have analysed the sequences of bacterial PDFs, including those of many pathogens, and identified two types, type I and type II. Here, we report the crystal structures of four different PDFs free or bound to actinonin from Gram-positive and Gram-negative bacteria, including two from the major bacterial pathogens,: type II PDFs from *S. aureus*, *Bacillus stearothermophilus*, type I PDFs from the *Pseudomonas aeruginosa* bacteria and type I *E. coli* PDF. These data allowed us to highlight the structural and molecular requirements for the design of a PDF inhibitor active against a broad spectrum of bacterial strains.

## Results

### Type I *versus* type II PDFs as revealed by amino acid sequence analysis

Using the many completed or nearly completed genomes of bacteria (>150), a systematic search for PDF sequences was undertaken using the specific features of the amino acid sequence already described.[28,32] The data reported in Figure 1 show that all bacterial genomes display one (e.g. *E. coli* or *S. aureus*), two (e.g. *P. aeruginosa* or *B. stearothermophilus*), three (e.g. *Shewanella putrefaciens*) or up to four (*Streptomyces coelicolor*) active PDF gene sequences. In addition to these PDF sequences, PDF homologs without deformylase activity have been described in *S. aureus* and *S. pneumoniae*.[8,33] Such homologs often occur in the genomes of other Gram-negative or Gram-positive bacteria (Rhizobiaceae, Streptococci, etc.) but were discarded systematically from the analysis shown in Figure 1. Although PDF have rather low levels of sequence similarity, the phylogenetic tree shown in Figure 1 reveals that they are closely related. This analysis highlights the occurrence of a distinct outgroup (coloured in red in Figure 1), which is more distant at the phylogenic level than the other sequences. This group occurs mainly in the Bacillus/Clostridium group of Gram-positive bacteria and is characterised at the sequence level by the presence of two insertions $I_1$ (two to five residues) and $I_2$ (11–13 residues) located in the N-terminal part of the protein around helix αA (Figure 2(a))[26] and by a hydrophobic C terminus. From this, two types of PDF amino acid sequence could be defined: type I and type II PDF. Many Gram-positive bacteria possess only one type II PDF, but Bacilli all have one type II and one type I PDF. Nevertheless, in *Bacillus* sp., it was demonstrated that the type II PDF was the major PDF and the main target of the specific antibiotic actinonin.[26,34] Note that all eukaryotic PDF belong to type I.[35] In order to assess the effect of the sequence diversity observed (i.e. of the type of PDF) on the 3D structure and its impact on inhibitor binding, two representative members of each type, *B. stearothermophilus1* and *S. aureus* for type II PDFs, and *P. aeruginosa1* and *E. coli* PDFs for type I PDFs, were selected for 3D structure determination and for studying the binding of specific inhibitors. It was verified that these four PDFs bind actinonin with similar potency.[36]

### Overall 3D structures

#### *E. coli* type I PDF

The crystals of *E. coli* PDF that have been grown are similar to those reported,[30,31] with three molecules of PDF per asymmetric unit and show highly identical structures.

**Figure 1**. A phylogenetic tree for bacterial PDF. PDF sequences were identified on the basis of three conserved motifs as described.[32,48] From more than 170 PDF sequences identified in several databases (http://www.ncbi.nlm.nih.gov/cgi-bin/Entrez/genom_table_cgi; http://www.sanger.ac.uk/DataSearch/omniblast.shtml), 120 sequences were selected as representative of the sequence diversity. The complete data set is available at http://www.isv.cnrs-gif.fr/TM/images/bacterialdef.txt. The sequences were aligned with ClustalX software,[49] the phylogenetic tree was constructed with N–J Tree[49] and drawn with TreeView1.65 (http://taxonomy.zoology.gla.ac.uk/rod/treeview.html).[50] Preliminary sequence data were obtained from (i) The Institute for Genomic Research website (http://www.tigr.org) or (ii) the Sanger Institute (ftp://ftp.sanger.ac.uk/pub/). Type I PDFs are coloured in green and type II PDFs are coloured in red.

(a)

```
                                        I1                                  I2      45
E.coli                  --SVLQVLHIPDERLRKVAKPVEE--VNAEIQRIVDDMFETMYAE----------EGIG
P.aeruginosa1           --AILNILEFPDPRLRTIAKPVEV--VDDAVRQLIDDMFETMYEA----------PGIG
S.aureus                MLTMKDIIRDGHPTLRQKAAELELPLTKEEKETLIAMREFLVNSQDEEIAKRYGLRSGVG
B.stearothermophilus1   MITMKDIIKEGHPTLRKVAEPVPLPPSEEDKRILQSLLDYVKMSQDPELAAKYGLRPGIG
                          ..  ..      **  *  .                                  *.*

                                                          I3                    98
E.coli                  LAATQVDIHQRIIVIDVSEN---RDERLVLINPELLEKSG---ETGIEEGCLSIP-EQRA
P.aeruginosa1           LAATQVNVHKRIVVMDLSED---KSEPRVFINPEFEPLTED--MDQYQEGCLSVP-GFYE
S.aureus                LAAPQINISKRMIAVLIPDDGSGKSYDYMLVNPKIVSHSVQEAYLPTGEGCLSVDDNVAG
B.stearothermophilus1   LAAPQINVSKRMIAVHVTDE-NGTLYSYALFNPKIVSHSVQQCYLTTGEGCLSVDRDVPG
                        *** *. . .*.. . . .            **     .          *****.

                                                                              158
E.coli                  LVPRAEKVKIRALDRDGKPFELEADGLLAICIQHEMDHLVGKLFMDYLSPLKQQRIRQKV
P.aeruginosa1           NVDRPQKVRIKALDRDGNPFEEVAEGLLAVCIQHECDHLNGKLFVDYLSTLKRDRIRKKL
S.aureus                LVHRHNRITIKAKDIEGNDIQLRLKGYPAIVFQHEIDHLNGVMFYDHIDKDHPLQPHTDA
B.stearothermophilus1   YVLRYARITVTGTTLDGEEVTLRLKGLPAIVFQHEIDHLNGIMFYDRINPADPFQVPDGA
                         * *  .. .     .*        *  *.  *** *** * .* * .      .

E.coli                  EKLDRLKARA
P.aeruginosa1           EKQHRQQA--
S.aureus                VEV-------
B.stearothermophilus1   IPIGR-----
```

(b)

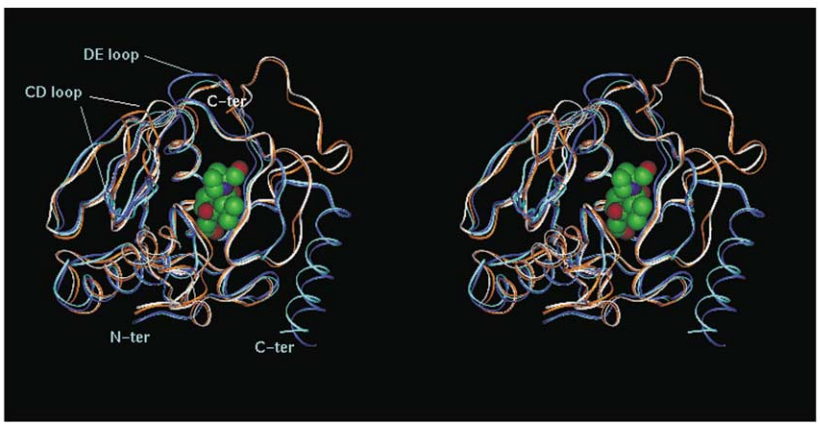


**Figure 2**. (a) Comparison between PDF structures. Structure based sequence alignment of *E. coli*, *B. stearothermophilus*, *S. aureus* and *P. aeruginosa* PDFs. Stars indicate conserved residues and dots mutations that preserve the nature of the amino acid residue. Boxes highlight residues that are located within 4.0 Å from the actinonin molecule (green for conserved residues and yellow for variable residues). The sequence identity between *E. coli* and *P. aeruginosa* PDF is 56%, 30% between *E. coli* and *B. stearothermophilus* and 23% between *E. coli* and *S. aureus*. *B. stearothermophilus* and *S. aureus* PDFs share a high level of sequence identity (54%) The insertions are denoted $I_1$, $I_2$ and $I_3$. (b) Overlay of the PDF structures. The ribbon diagrams are shown for *E. coli* (cyan), *B. stearothermophilus* (white), *S. aureus* (orange) and *P. aeruginosa* (dark blue) PDFs. Actinonin when bound to *B. stearothermophilus* PDF is displayed as a CPK model with carbon atoms green, oxygen atoms red and nitrogen atoms blue.

### *P. aeruginosa* type I PDF

The overall structure of *P. aeruginosa* when complexed with actinonin is essentially similar to that observed for the *E. coli* complex, as indicated by the r.m.s.d. value of 1.0 Å for 159 out of 164 $C^{\alpha}$ atoms (Figure 2(b)). However, some structural differences are observed in three areas: (i) the CD loop; (ii) the DE loop and its flanking β strands; and (iii) for the C-terminal helix. The CD loop in *E. coli* was observed to show some conformational variability in the three copies found in the asymmetric unit of the crystal. Maximum shifts of about 3.3 Å are observed for the $C^{\alpha}$ atom of residue R66 within the CD loop. The DE loop corresponds to a region with no sequence identity between these enzymes and where a single amino acid insert occurs in *P. aeruginosa*. This has resulted in some significant structural rearrangements. The flanking βD strand is displaced and shifts of about 4.0 Å are observed for residue L78. The DE loop adopts a completely different conformation and the first residues of the βE strand are affected by these shifts. The αJ helix appears to be canted at a slightly different angle with respect to the rest of the structure when compared with *E. coli*. This

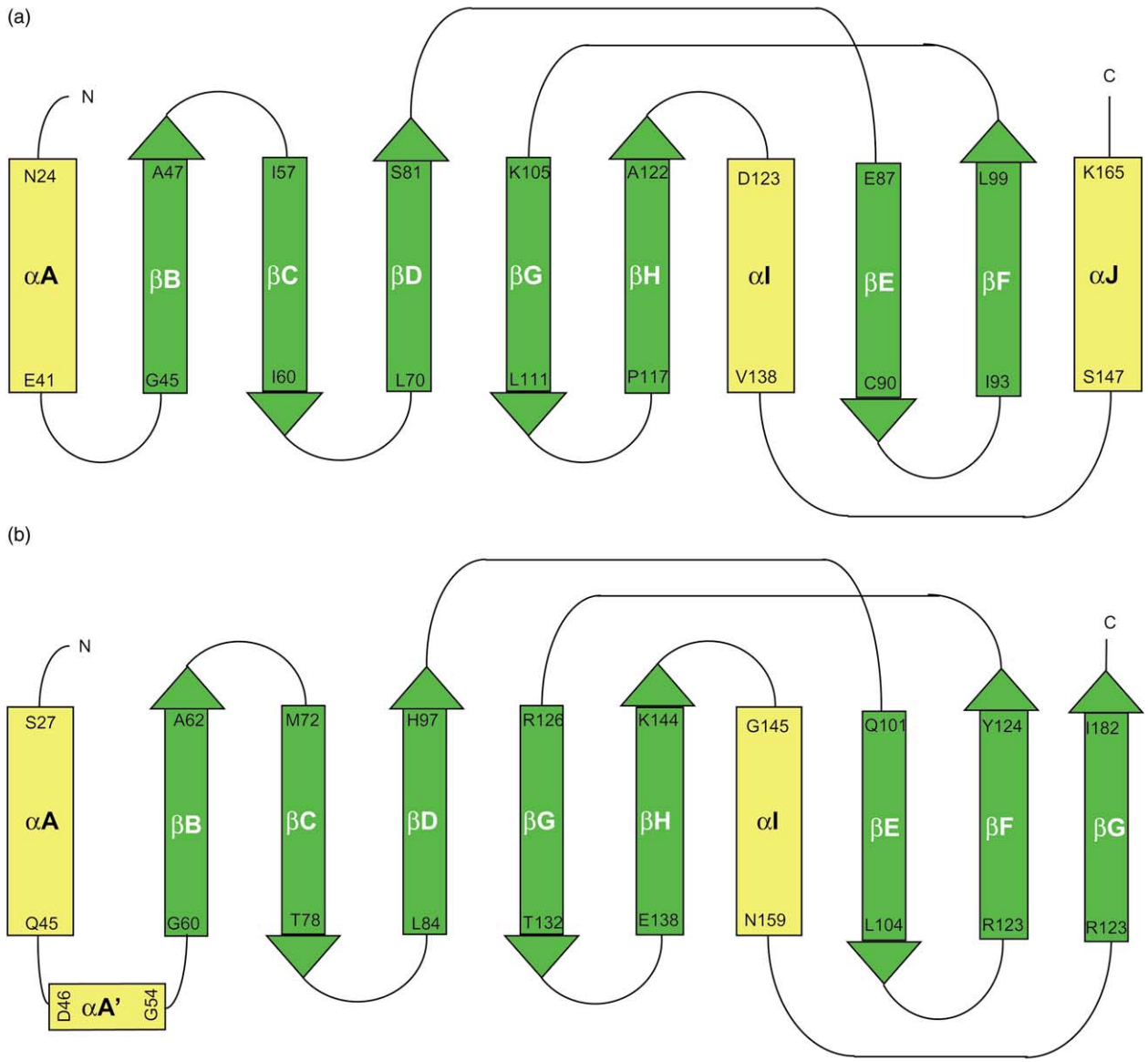


**Figure 3**. The topological diagram of PDF for (a) Gram-negative bacteria and for (b) Gram-positive bacteria is shown. The residue numbers that are given correspond to those of (a) *E. coli* and(b) *B. stearothermophilus* PDF helices are shown with yellow rectangles and strands with green helices. Secondary structure elements were determined with the program PROMOTIF.[51]

is likely a result of the differences in side-chain atoms in the αJ helix that make contacts with the rest of the protein. These three areas lie far away from the catalytic site.

### *B. stearothermophilus* type II PDF

The overall structure of *B. stearothermophilus* PDF is similar to that of *E. coli* but with only 113 $C^{\alpha}$ atoms out of 166 superimposing with an r.m.s.d. of 0.8 Å compared with the 159 $C^{\alpha}$ atoms from *P. aeruginosa* that can be fitted (Figure 2(b)). These atoms correspond to the $C^{\alpha}$ positions of elements of secondary structure. However, there are some significant structural differences: the αA helix appears to be canted at a different angle when compared with *E. coli*. The 11 residue $I_2$ insertion in the AB loop folds into a short two-turn α-helix termed αA′ facing towards the solvent and that is not involved in ligand binding. The CD loop that differs in sequence and in length not surprisingly differs also in structure. The main striking difference lies in the C-terminal area: the terminal α-helix that is found in both *E. coli* and *P. aeruginosa* PDFs is not observed in this structure. It is replaced by a loop followed by a small β-strand termed βH, which folds back on the small second β-sheet, making hydrogen bond interactions with the βF strand. Interestingly, the polypeptide chain after residue P148 of this type II PDF runs in the direction opposite to that observed for *E. coli* and *P. aeruginosa* PDFs. This absence of the C-terminal

α-helix is not due to crystal packing, as it is observed in another crystal form (data not shown). The absence of the terminal helix has induced some changes in the position and conformation of the long EF loop. In both *E. coli* and *P. aeruginosa* PDFs, this loop was sandwiched between the central αI and the terminal αJ helix. In the case of the *B. stearothermophilus* PDF, the EF loop is also nestled against the central helix but is not covered up by any element of secondary structure, providing a much more relaxed conformation. This has induced a significant enlargement of the S2′ pocket. Hence, the EF loop of *B. stearothermophilus* PDF resembles more closely that observed in the structure of the *E. coli* enzyme devoid of the terminal αJ helix.[26]

### *S. aureus* type II PDF

The overall structure is very similar to that of *B. stearothermophilus* PDF with 179 $C^{\alpha}$ atoms out of 183 superimposing with an r.m.s.d. of 0.9 Å and consequently shows some significant differences when compared to *E. coli* and *P. aeruginosa* PDFs. Likewise, in *B. stearothermophilus* PDF the terminal α-helix visible in both *E. coli* and *P. aeruginosa* is not observed in this PDF but instead a loop is followed by a small β-strand (Figure 3).

### Metal-binding site

The *E. coli* and *P. aeruginosa* PDFs were purified in the presence of zinc, whereas the *B. stearothermophilus* PDF was prepared in the presence of nickel. The metal content of these three PDFs was assessed by atomic absorption spectrometry, unlike that of *S. aureus* which was used for the crystallographic study and was not fully characterised. However the low activity of the *S. aureus* enzyme and the absence of anomalous signal found in the Patterson map suggest that $Zn^{2+}$ is the most likely metal and consequently it was fitted into the electron density and retained throughout refinement. From these four structures, it appears that, regardless of the nature of the cation and of the bacterial strain, the three residues H132, H136 and C90 that participate in the metal coordination adopt highly conserved conformations, as shown in Figure 4(b). This is in keeping with the observation made with the $Fe^{2+}$, $Ni^{2+}$ and $Zn^{2+}$ forms of the *E. coli* enzyme.[26,30] In addition residues such as Gln50 or Glu133 that presumably participate in catalysis are structurally perfectly conserved.

### Catalytic site

For *E. coli* PDF, it was shown that the binding site of actinonin was a deep invagination made by residues from the central helix αI and from the strands βB and βE. Sixteen residues from the *E. coli* PDF are located within 4.0 Å from actinonin and include G43, I44, G45, L46, Q50, E88, G89, C90, L91, R97, L125, I128, C129, H132, E133 and H136. Two additional residues were found in *P. aeruginosa* and in *B. stearothermophilus* to lie within 4.0 Å from actinonin (I86 and E87). Taken together, these 18 residues define the binding site. Four residues out of the 18 from the active site are not conserved in *P. aeruginosa*, four in *B. stearothermophilus* and six in *S. aureus* PDF (Figure 4). The r.m.s.d. for the 14 conserved residues and for the equivalent atoms from the four variable residues is 0.6 Å, indicating an identical binding site for *P. aeruginosa* PDF. The corresponding values for *B. stearothermophilus* and *S. aureus* are 1.3 Å and 1.7 Å, respectively, suggesting an overall conserved binding site with some differences. Taken together, seven residues including I44, I86, E87, R97, L125, I128 and C129, are not conserved within the active site (Figure 4). They contribute to the delineation of the S1′ (I128, I86, C129, I44) and S3′ (I86, L125, E87, R97) pockets. The variable residues found in the S1′ cleft modify its overall shape only slightly, while retaining an overall hydrophobic character. In contrast, mutations in the S3′ pocket change its chemical nature and they induce a significant change of its shape (Figure 4).

The conformations of bound actinonin are very conserved for the three complexes for which a structure has been determined, as typified by an r.m.s.d. of 0.6 Å for all atoms that bind actinonin when comparing *E. coli* and *P. aeruginosa* PDFs (Figure 5). The corresponding comparison between *E. coli* and *B. stearothermophilus* PDF-bound actinonin yields a similar value of 0.5 Å. Slight differences observed for the alkyl chain in the P1′ position are unlikely to be significant. The interactions between actinonin and *E. coli* PDF have been described:[37] the hydroxamate group provides a perfect bidentate ligand to the $Zn^{2+}$ with the carbonyl and hydroxyl oxygen atoms while the nitrogen atom establishes strong H-bonds with the carboxylate group of E133 and the carbonyl oxygen atom of G45. In addition to the hydroxamate atoms, all other polar atoms from actinonin are within range of strong H-bond interactions with PDF main-chain atoms, except the amide nitrogen atom of the valine residue that lies at about 3.2 Å from the carbonyl oxygen atom of G89: the carbonyl oxygen atom of the pentyl succinate group is involved in H-bond interaction with the amide nitrogen atom of I44 and the valine amide group of actinonin contacts the G89 amide group. The interaction between actinonin and PDF can be envisioned as a bridge between the two sheets, connecting strands βB and βE. The mode of binding between actinonin and *P. aeruginosa* and *B. stearothermophilus* PDFs are very similar. Some minor differences are found in the *B. stearothermophilus* PDF/actinonin complex: the hydroxamate moiety bridges the amido group of Q50, the side-chain atoms of the L-prolinol group make van der Waals contacts with L104 and its hydroxyl group is involved in a H-bond

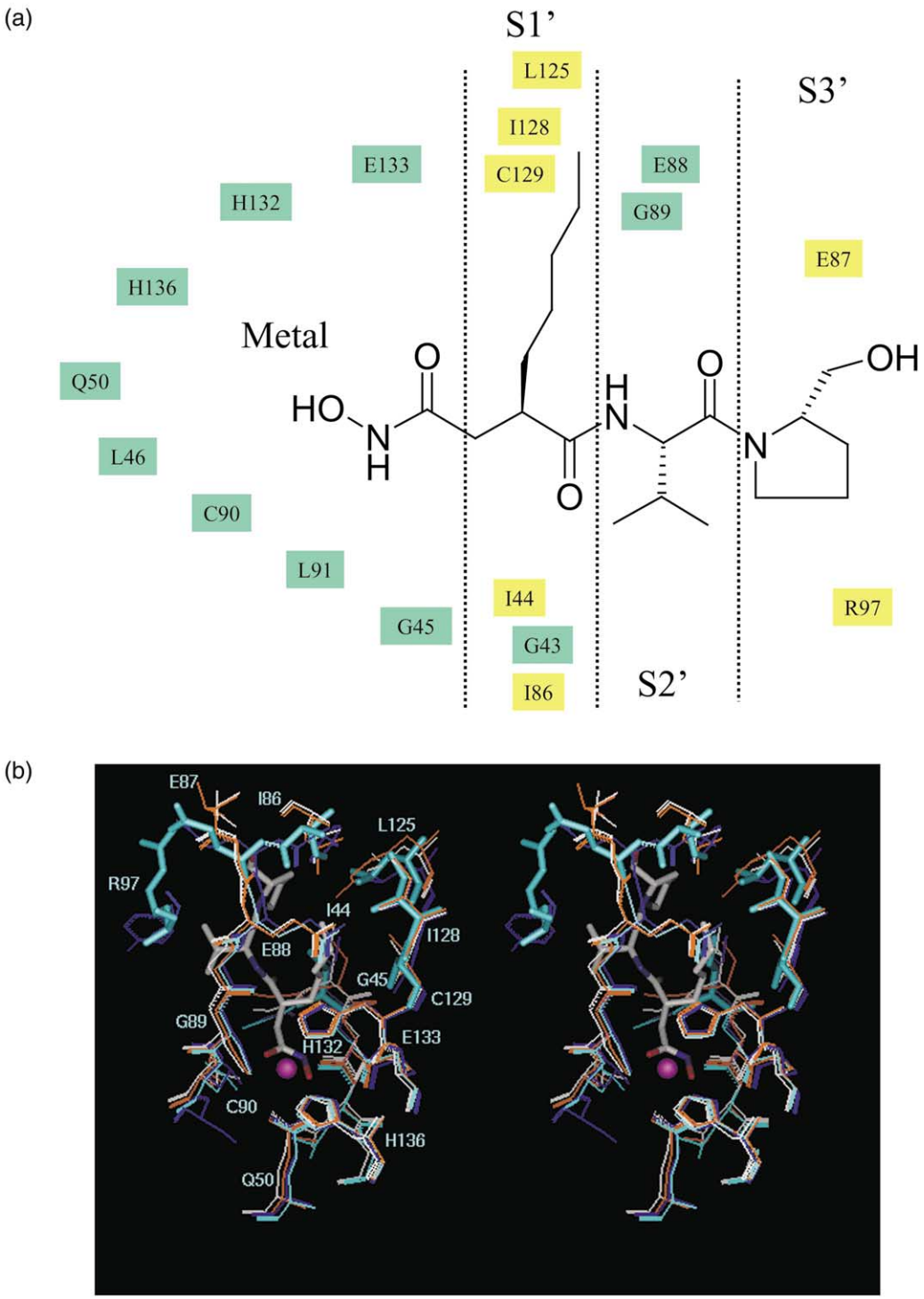


**Figure 4**. (a) Comparison of the active site of PDF. Molecular structure of actinonin and delineation of the sub-sites of the binding pocket. Residues highlighted in green correspond to conserved residues and in yellow to variable residues within the four PDF studied (see also Figure 2). (b) Comparison of the binding sites. The proteins are displayed with a line model where the metal ion is shown as a magenta ball, nitrogen, oxygen and sulfur atoms are represented in blue, red and yellow, respectively. The carbon atoms are shown for *E. coli* in cyan, *B. stearothermophilus* in white, *S. aureus* in orange and *P. aeruginosa* in dark blue. Variable residues are shown with a ball-and-stick model. Numbering corresponds to that of *E. coli* PDF.

contact with T106 from *B. stearothermophilus* PDF (Figure 5). These latter additional contacts result from the presence of the EF loop that displays a conformation different from that in *E. coli* PDF (see above).

## Discussion

The structures reported here show that the overall 3D topology of PDF is conserved amongst the various bacterial strains studied, as are the active

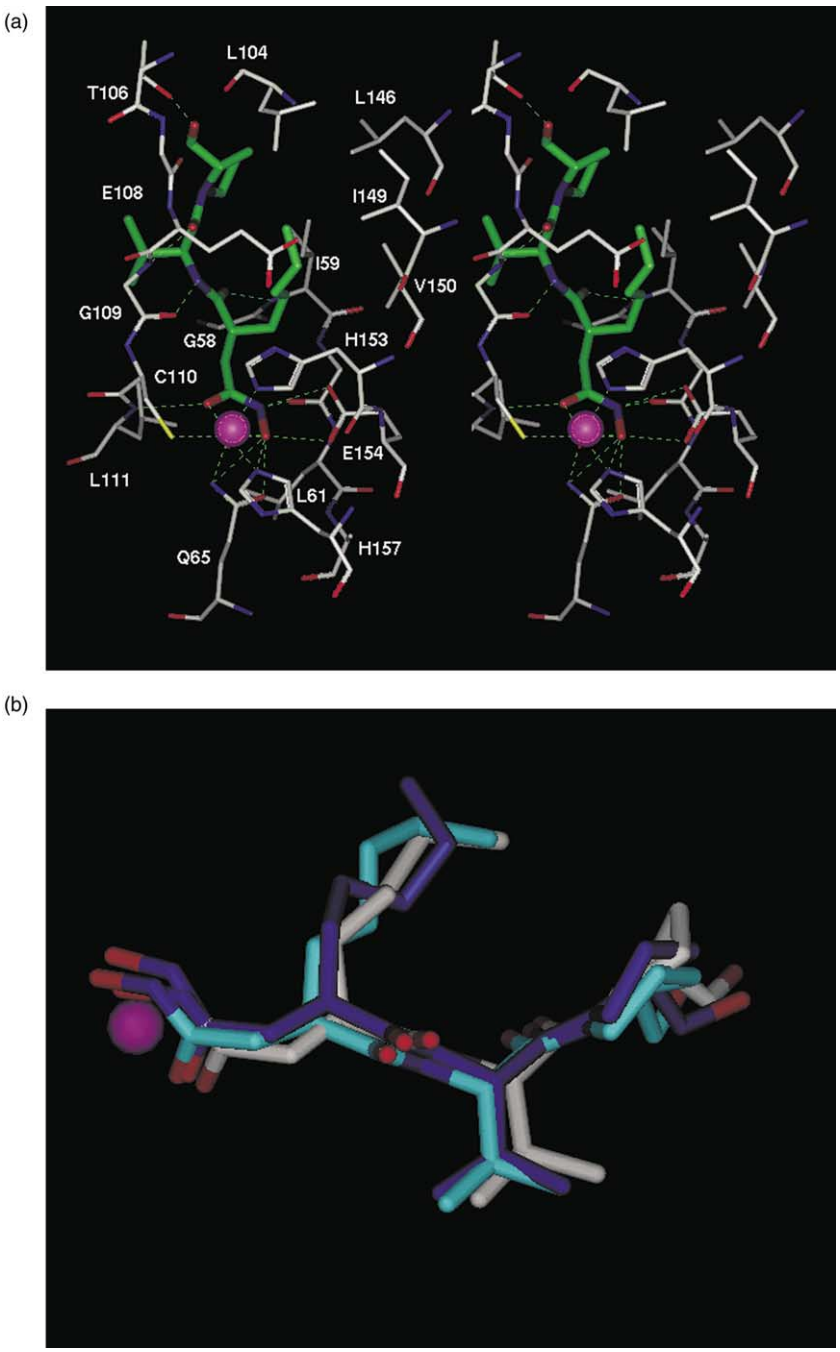


**Figure 5**. Binding mode of actinonin. (a) Binding mode of actinonin to *B. stearothermophilus* PDF. Protein is displayed using a line model with carbon, nitrogen, oxygen and sulfur atoms shown in white, blue, red and yellow, respectively. The actinonin molecule is represented with its carbon atoms in green. Dotted lines correspond to H-bonds. The numbering of residues corresponds to that of *B. stearothermophilus* PDF. (b) Overlay of the bound conformation of actinonin to various PDFs with carbon atoms of *E. coli* in cyan, *B. stearothermophilus* in white, and *P. aeruginosa* in dark blue. The superimposition results from the overlay made with the protein atoms.

site and the binding mode of the pseudopeptide-like substrate actinonin. In addition, no significant structural change is observed upon binding. The sequence alignment of a variety of PDFs has suggested a clear separation into two types within bacteria, which does not fully reflect the distinction between Gram-negative and Gram-positive bacteria. This two-type classification is now confirmed at the 3D level, where significant structural differences are observed mainly at the C terminus. As fully expected from its amino acid sequence, the 3D structure of the *P. falciparum* PDF shows that it belongs to type I PDFs.[29,32,35] The C-terminal helix observed for type I PDFs is replaced in type II PDFs by a long loop followed by a small β-strand that folds back on the second β-sheet. In addition, type II PDFs have a supplementary α-helix inserted in the AB loop. This change of secondary structure has not affected the conformation of the catalytic site, although significant enlargement of the S2′ site is observed, indicating that compounds that contain significantly large P2′ groups are likely to be specific against the type I PDFs. Nevertheless, the catalytic properties of

**Table 1.** Crystal and diffraction data

| | *E. coli* | *E. coli* + EMTS | *P. aeruginosa* | *S. aureus* | *B.stearothermophilus* |
|---|---|---|---|---|---|
| A. *Crystal parameters* | | | | | |
| Initial drop composition | 4 μl, 25 mM Mes–NaOH (pH 6.0), 1.0 M $(NH_4)_2SO_4$, 0.5 mM protein, 0.5 mM actinonin | 4 μl, 25 mM Mes–NaOH (pH 6.0), 1.0 M $(NH_4)_2SO_4$, 0.5 mM protein, 1 mM EMTS | 4 μl, 30 mM Caps–HCl (pH 9.5), 16% $PEG_{6000}$, 0.6 mM protein, 0.6 mM actinonin | 4 μl, 1.04 M $K_2HPO_4$/$NaH_2PO_4$ (pH 4.8), 0.65 mM protein | 4 μl, 25 mM Hepes–HCl (pH 7.5), 3.5% $PEG_{6000}$, 0.7 mM protein, 0.7 mM actinonin |
| Well composition | 1 ml, 50 mM Mes–NaOH (pH 6.0), 2.0 M $(NH_4)_2SO_4$ | 1 ml, 50 mM Mes–NaOH (pH 6.0), 2.0 M $(NH_4)_2SO_4$ | 1 ml, 60 mM Caps–HCl (pH 9.5), 32% $PEG_{6000}$ | 1 ml, 2.08 M $K_2HPO_4$/$NaH_2PO_4$ (pH 4.8) | 50 mM Hepes–HCl (pH 7.5), 7% $PEG_{6000}$ |
| Cryoprotectant solution composition | 50 mM Mes–NaOH (pH 6.0), 0.5 M $(NH_4)_2SO_4$, 28% $PEG_{400}$ | 50 mM Mes–NaOH (pH 6.0), 0.5 M $(NH_4)_2SO_4$, 28% $PEG_{400}$ | 25% $PEG_{6000}$, 25% $PEG_{400}$, 50 mM Caps–HCl (pH 9.5) | 0.2 M $K_2HPO_4$/$NaH_2PO_4$ (pH 4.8), 25% $PEG_{400}$, 25% $PEG_{400}$ | 50 mM Hepes–HCl (pH 7.5), 25% $PEG_{400}$ |
| Space group | *C*2 | *C*2 | $P2_12_12_1$ | $P2_1$ | $P2_12_12_1$ |
| Cell dimensions *a*, *b*, *c* (Å) | 141.0, 63.6, 83.5 | 139.0, 63.0, 84.8 | 50.4, 60.1, 73.2 | 48.2, 42.2, 101.7 | 42.0, 43.1, 92.2 |
| α, γ, β (deg.) | 90.0, 90.0, 123.35 | 90.0, 90.0, 121.7 | 90.0, 90.0, 90.0 | 90.0, 90.0, 98.7 | 90.0, 90.0, 90.0 |
| B. *Diffraction data* | | | | | |
| X-ray source | Cu Kα rotating anode | Cu Kα rotating anode | Cu Kα rotating anode | ESRF, ID14-EH3 | Cu Kα rotating anode |
| $R_{sym}$[a] (%) | 7.6 (25.1) | 7.3 (27) | 8.8 (24.6) | 4.6 (27.4) | 3.9 (8.3) |
| Completeness[a] (%) | 93.7 (83.7) | 92.5 (67.9) | 85.5 (85.3) | 98.5 (95.4) | 98.0 (95.3) |
| Resolution (Å) | 2.1 | 2.5 | 2.6 | 1.87 | 1.9 |
| $I/\sigma(I)$[a] | 18.3 (5.0) | 8.1 (2.2) | – | 9.8 (2.3) | 24.7 (12.8) |
| No. reflections | 34,394 | 20,212 | 7756 | 33,121 | 13,516 |
| Redundancy | 2.4 | 2.1 | 2.7 | 2.5 | 2.9 |

EMTS, ethylmercurylthiosalicylate.
[a] Data in the last resolution shell are given in parentheses.

these PDFs are very similar, showing that the differences in 3D structure have no significant functional consequences.[18,28]

Some residues from the binding site of the substrate-like inhibitor actinonin are conserved in sequence and in spatial position. They correspond to the amino acid residues that are involved either in the metal coordination or in the interactions with the peptide amide bonds or with the *n*-pentyl chain. This is consistent with the fact that PDF is required to process all nascent formylated polypeptides starting with methionine regardless of the identity of the amino acid residues found in positions P2′ and P3′. This has some strong implications for the design of PDF inhibitors directed against a broad set of bacterial pathogens. Compounds for which the binding affinity derives from significant contacts with other areas are unlikely to target a large spectrum of PDFs. In addition, resistant strains are likely to emerge with mutations of the *def* gene in these variable areas that retain the catalytic efficiency of the enzyme and that provide a survival mechanism for the bacterium to the treatment with this type of PDF inhibitor.[38] The actinonin molecule fits snugly into the catalytic pocket of PDF, highlighting the small size of the active site. This would suggest that the scope for designing structurally diverse potent broad-spectrum inhibitors of PDF is presumably rather limited and that most highly active compounds will consist mainly of (i) a small metal-chelating group, (ii) a hydrophobic saturated alkyl chain to fit into the S1′ cleft, and (iii) two amide bonds to participate in H-bond interactions with the two βB and βE strands.[12,36] This is exemplified by the pseudopeptide compounds reported recently that display nanomolar activity *in vitro*.[37,39,40] Peptide-like molecules are usually not considered very attractive for drug development because of their poor pharmacokinetic properties. Interestingly, however, some of the compounds described exhibit some significant oral bio-availability in a mouse model.[37]

To conclude, this work shows that, regardless of the type, PDFs display conserved active sites and binding modes to actinonin despite some

**Table 2.** Results of structure refinement

| | *E. coli* | *P. aeruginosa* | *S. aureus* | *B. stearothermophilus* |
|---|---|---|---|---|
| No. reflections (total) | 34,376 | 7747 | 32,301 | 13,368 |
| No. reflections (used for refinement) | 34,376 | 7747 | 30,645 | 12,423 |
| No. reflections (used for *R*-free) | 0 | 0 | 1656 | 942 |
| No. protein atoms (occupancy⟨⟩0) | 3882 | 1333 | 2875 | 1433 |
| No. ligand atoms | 81 | 27 | – | 27 |
| No. metal atoms | 3 | 1 | 1 | 2 |
| No. solvent molecules | 486 | 150 | 175 | 261 |
| Average *B*-value for protein atoms (Å$^2$) | 26.0 | 17.8 | 27.3 | 12.0 |
| *B*-Value for ligand/metal atoms (Å$^2$) | 22.8/20.5 | 22.6/21.2 | –/30.0 | 10.2/22.2 |
| Average *B*-value for the solvent molecules (Å$^2$) | 33.4 | 30.2 | 37.2 | 27.6 |
| Range of spacings (Å) | 15.0–2.1 | 15.0–2.6 | 100–1.87 | 19.0–1.9 |
| *R*-value | 0.24 | 0.221 | 0.231 | 0.161 |
| *R*-free (% reserved) | –(0) | –(0) | 0.265 (5) | 0.242 (7) |
| Weighted r.m.s.d. from ideality | | | | |
| Bond length (Å) | 0.012 | 0.007 | 0.012 | 0.017 |
| Bond angle (deg.) | 1.8 | 1.5 | 1.65 | 1.705 |

significant structural differences at the C terminus. It has enabled us to identify a small number of conserved amino acid residues of PDF at the 3D level that would appear critical for productive binding, providing clear but limited avenues to develop highly potent broad-spectrum PDF inhibitors. Recently, it has been shown that a significantly high frequency of mutations is observed in *S. aureus* strains treated with a PDF inhibitor.[8] Taken together with the structural data, this suggests that the development of a PDF inhibitor for human treatment targeting a reduced spectrum of bacteria is more likely to succeed.

## Materials and Methods

### Notation

The numbering follows that of *E. coli* PDF. The standard nomenclature used in the protease field[41] to designate substrate/inhibitor residues (P2, P1, P1′, P2′, P3′) that bind to the corresponding enzyme sub-sites is shown in Figure 4.

### Isolation and purification

*E. coli* and *B. stearothermophilus* PDFs were purified as described.[15,18] *S. aureus* and *P. aeruginosa* PDFs were cloned by PCR, using degenerated primers, designed from conserved amino acid motifs, determined by comparison of three PDFs: *E. coli*, *Haemophilus influenzae* and *Thermus thermophilus*.[28] For *S. aureus*, the conserved motifs used were GVGLAAPQ and QHEIDHL. The PCR was performed with total DNA extracted from the *S. aureus* RN4220, and a 350 bp fragment corresponding to *S. aureus* PDF was cloned and sequenced. Using this fragment as a probe, the complete nucleotide sequence from *S. aureus* PDF was then isolated from a *S. aureus* RN4220 genomic library. For *P. aeruginosa*, the conserved motifs used were GIGLAAPQ and QHEMDHL. The PCR was performed with total DNA extracted from *P. aeruginosa* ATCC27853, and two different 300 bp fragments were cloned and sequenced. Both displayed homology with other PDFs. Using these fragments as probes, the complete nucleotide sequence for the two *P. aeruginosa* PDFs were then isolated from two different clones from a *P. aeruginosa* ATCC27853 genomic library. The X-ray structure presented in this paper corresponds to the *P. aeruginosa* PDF located upstream of the formyltransferase gene (*fmt*) and which displayed the highest homology to the *E. coli* PDF. It was shown that both *P. aeruginosa* PDFs were active as they were both able to complement the *E. coli* Δ*def* (Pal421Tr-pMAK) strain.[7] All purification steps were carried out at 4 °C for *S. aureus* and *P. aeruginosa*. 20 g (wet weight) of *S. aureus* pellet were lysed by sonication treatment (30 minutes) in lysis buffer A (50 mM bis-tris-propane (pH 7.5), 1 mM DTT, 150 mM NaCl, 10% (v/v) glycerol). The lysate was spun at 30,000 ***g*** for 60 minutes. The supernatant was desalted through PD10 columns equilibrated in buffer A without NaCl to obtain approximately 2 g of proteins. Supernatant was then loaded onto a MONO Q HR 10/10 column (AP-Biotech) equilibrated in buffer B (20 mM bis-tris-propane (pH 7.5), 0.5 mM DTT and eluted with two 20 minute linear gradients (0 mM to 100 mM KCl, then 100 mM to 500 mM KCl in buffer B). Active fractions were pooled and concentrated through Centriprep 10 concentrators (Amicon) and further purified by gel-filtration using a Superdex 75 HR 26/60 column (AP-Biotech) equilibrated in buffer C (50 mM Hepes (pH 7.5), 250 mM NaCl). The purity of active fractions was checked by denaturing electrophoresis. Homogeneous fractions (95 mg of protein) were pooled. PDF from *P. aeruginosa* was purified using the same procedure. PDF activity was monitored using formyl-Met-Ala-Ser as a substrate and ninhydrin revelation as described.[24] Protein concentrations were measured according to Bradford[42] using bovine serum albumin as a protein standard.

### Data collection and processing

Crystals were grown by vapor-diffusion at 19 °C by the hanging-drop method. Crystallization conditions are given in Table 1. All crystals were picked up with a fibre loop and flash-cooled in a stream of gaseous nitrogen at 100 K. The X-ray intensity data were collected either on a DIP2000 imaging plate (Mac Sciences, Japan) mounted on a FR591 rotating anode with Frank's double focusing mirrors (Nonius, The Netherlands), operated at 50 kV, 90 mA or at the ESRF on beamline ID14-EH3. Data processing and scaling was carried out using either

DENZO and SCALEPACK[43] or MOSFLM and SCALA (CCP4[44]). Crystal data are presented in Table 1.

### Structure solution and crystallographic refinement

The structure of *E. coli* deformylase was solved by the SIRAS method because at the time no crystal structure of PDF was publicly available. A single ethylmercurylthiosalicylate (EMTS) derivative with the anomalous signal provided enough phasing power to generate useful phases (phasing power of 1.36 and 1.82 for the isomorphous and anomalous cases, respectively and $R_{cullis}$ of 0.64 for centric reflections). Refinement of the heavy-atom phases was carried out with SHARP[45] followed by solvent flattening, this yielded an interpretable electron density map. Model building was carried out with O[46] and subsequent crystallographic refinement was performed with X-PLOR.[47] Other deformylase structures were readily solved by molecular replacement using a pruned model derived from *E. coli* PDF and refined to acceptable statistics that are shown in Table 2.

### Protein Data Bank accession codes

Atomic coordinates have been deposited with the Rcsb Protein Data Bank, with accession codes 1LQW, 1LQY, 1LRY, and 1LRU.

## Acknowledgments

We thank S. Ross for proof-reading the manuscript. J.-M. Paris, D. Thibaut, J.-D. Guitton, C. Carrez and E. James are gratefully acknowledged for constant support. C. Lazennec is acknowledged for help with the initial stage of crystallization of the *B. stearothermophilus* enzyme. Preliminary sequence data were obtained from The Institute for Genomic Research website at http://www.tigr.org

## References

1. Meinnel, T., Mechulam, Y. & Blanquet, S. (1993). Methionine as translation start signal: a review of the enzymes of the pathway in *Escherichia coli*. *Biochimie*, **75**, 1061–1075.
2. Adams, J. M. (1968). On the release of the formyl group from nascent protein. *J. Mol. Biol.* **33**, 571–589.
3. Livingston, D. M. & Leder, P. (1969). Deformylation and protein synthesis. *Biochemistry*, **8**, 435–443.
4. Takeda, M. & Webster, R. E. (1968). Protein chain initiation and deformylation in *B. subtilis* homogenates. *Proc. Natl Acad. Sci. USA*, **60** 1487–1494.
5. Guillon, J. M., Heiss, S., Soutourina, J., Mechulam, Y., Laalami, S., Grunberg-Manago, M. & Blanquet, S. (1996). Interplay of methionine tRNAs with translation elongation factor Tu and translation initiation factor 2 in *Escherichia coli*. *J. Biol. Chem.* **271**, 22321–22325.
6. Mazel, D., Pochet, S. & Marliere, P. (1994). Genetic characterization of polypeptide deformylase, a distinctive enzyme of eubacterial translation. *EMBO J.* **13**, 914–923.
7. Meinnel, T. & Blanquet, S. (1994). Characterization of the *Thermus thermophilus* locus encoding peptide deformylase and methionyl-tRNA(fMet) formyltransferase. *J. Bacteriol.* **176**, 7387–7390.
8. Margolis, P. S., Hackbarth, C. J., Young, D. C., Wang, W., Chen, D., Yuan, Z. *et al.* (2000). Peptide deformylase in *S. aureus*: resistance to inhibition is mediated by mutations in the formyltransferase gene. *Antimicrob. Agents Chemother.* **44**, 1825–1831.
9. Apfel, C. M., Locher, H., Evers, S., Takacs, B., Hubschwerlen, C., Pirson, W. *et al.* (2001). Peptide deformylase as an antibacterial drug target: target validation and resistance development. *Antimicrob. Agents Chemother.* **45**, 1058–1064.
10. Giglione, C., Serero, A., Pierre, M., Boisson, B. & Meinnel, T. (2000). Identification of eukaryotic peptide deformylases reveals universality of N-terminal protein processing mechanisms. *EMBO J.* **19**, 5916–5929.
11. Serero, A., Giglione, C. & Meinnel, T. (2001). Distinctive features of the two classes of eukaryotic peptide deformylases. *J. Mol. Biol.* **314**, 695–708.
12. Giglione, C., Pierre, M. & Meinnel, T. (2000). Peptide deformylase as a target for new generation, broad spectrum antimicrobial agents. *Mol. Microbiol.* **36**, 1197–1205.
13. Pei, D. (2001). Peptide deformylase: a target for novel antibiotics? *Emerg. Therap. Targets*, **5**, 23–40.
14. Yuan, Z., Trias, J. & White, R. J. (2001). Deformylase as a novel antibacterial target. *Drug Discov. Today*, **6**, 954–961.
15. Meinnel, T. & Blanquet, S. (1995). Enzymatic properties of *Escherichia coli* peptide deformylase. *J. Bacteriol.* **177**, 1883–1887.
16. Groche, D., Becker, A., Schlichting, I., Kabsch, W., Schultz, S. & Wagner, A. F. (1998). Isolation and crystallization of functionally competent *Escherichia coli* peptide deformylase forms containing either iron or nickel in the active site. *Biochem. Biophys. Res. Commun.* **246**, 342–346.
17. Rajagopalan, P. T. R., Yu, X. C. & Pei, D. (1997). Peptide deformylase: a new type of mononuclear iron protein. *J. Am. Chem. Soc.* **119**, 12418–12419.
18. Ragusa, S., Blanquet, S. & Meinnel, T. (1998). Control of peptide deformylase activity by metal cations. *J. Mol. Biol.* **280**, 515–523.
19. Rajagopalan, P. T., Grimme, S. & Pei, D. (2000). Characterization of cobalt(II)-substituted peptide deformylase: function of the metal ion and the catalytic residue Glu-133. *Biochemistry*, **39**, 791–799.
20. Gordon, J. J., Kelly, B. K. & Miller, G. A. (1962). Actinonin: an antibiotic substance produced by an actinomycete. *Nature*, **195**, 701–702.
21. Gordon, J. J., Devlin, J. P., East, A. J., Ollis, W. D., Sutherland, I. O., Wright, D. E. & Ninet, L. (1975). Studies concerning the antibiotic actinonin. Part I. The constitution of actinonin. A natural hydroxamic acid with antibiotic activity. *J. Chem. Soc., Perkin Trans. 1*, **9**, 819–825.
22. Lelievre, Y., Bouboutou, R., Boiziau, J. & Cartwright, T. (1989). Inhibition of synovial collagenase by actinonin. Study of structure/activity relationship. *Pathol. Biol. (Paris)*, **37**, 43–46.
23. Chen, D. Z., Patel, D. V., Hackbarth, C. J., Wang, W., Dreyer, G., Young, D. C. *et al.* (2000). Actinonin, a naturally occurring antibacterial agent, is a potent deformylase inhibitor. *Biochemistry*, **39**, 1256–1262.
24. Meinnel, T., Lazennec, C. & Blanquet, S. (1995). Mapping of the active site zinc ligands of peptide deformylase. *J. Mol. Biol.* **254**, 175–183.

25. Ragusa, S., Mouchet, P., Lazennec, C., Dive, V. & Meinnel, T. (1999). Substrate recognition and selectivity of peptide deformylase. Similarities and differences with metzincins and thermolysin. *J. Mol. Biol.* **289**, 1445–1457.
26. Dardel, F., Ragusa, S., Lazennec, C., Blanquet, S. & Meinnel, T. (1998). Solution structure of nickel-peptide deformylase. *J. Mol. Biol.* **280**, 501–513.
27. Meinnel, T., Lazennec, C., Dardel, F., Schmitter, J. M. & Blanquet, S. (1996). The C-terminal domain of peptide deformylase is disordered and dispensable for activity. *FEBS Letters*, **385**, 91–95.
28. Meinnel, T., Lazennec, C., Villoing, S. & Blanquet, S. (1997). Structure–function relationships within the peptide deformylase family. Evidence for a conserved architecture of the active site involving three conserved motifs and a metal ion. *J. Mol. Biol.* **267**, 749–761.
29. Kumar, A., Nguyen, K. T., Srivathsan, S., Ornstein, B., Turley, S., Hirsh, I. *et al.* (2002). Crystals of peptide deformylase from *Plasmodium falciparum* reveal critical characteristics of the active site for drug design. *Structure (Camb)*, **10**, 357–367.
30. Becker, A., Schlichting, I., Kabsch, W., Groche, D., Schultz, S. & Wagner, A. F. (1998). Iron center, substrate recognition and mechanism of peptide deformylase. *Nature Struct. Biol.* **5**, 1053–1058.
31. Chan, M. K., Gong, W., Rajagopalan, P. T., Hao, B., Tsai, C. M. & Pei, D. (1997). Crystal structure of the *Escherichia coli* peptide deformylase. *Biochemistry*, **36**, 13904–13909. [Published erratum appears in Biochemistry 1998 Sep 15, **37**(37), 13042].
32. Meinnel, T. (2000). Peptide deformylase of eukaryotic protists: a target for new antiparasitic agents? *Parasitol. Today*, **16**, 165–168.
33. Margolis, P., Hackbarth, C., Lopez, S., Maniar, M., Wang, W., Yuan, Z. *et al.* (2001). Resistance of *Streptococcus pneumoniae* to deformylase inhibitors is due to mutations in defB. *Antimicrob. Agents Chemother.* **45**, 2432–2435.
34. Haas, M., Beyer, D., Gahlmann, R. & Freiberg, C. (2001). YkrB is the main peptide deformylase in *Bacillus subtilis*, a eubacterium containing two functional peptide deformylases. *Microbiology*, **147**, 1783–1791.
35. Giglione, C. & Meinnel, T. (2001). Organellar peptide deformylases: universality of the N-terminal methionine cleavage mechanism. *Trends Plant Sci.* **6**, 566–572.
36. Meinnel, T., Patiny, L., Ragusa, S. & Blanquet, S. (1999). Design and synthesis of substrate analogue inhibitors of peptide deformylase. *Biochemistry*, **38**, 4287–4295.
37. Clements, J. M., Beckett, R. P., Brown, A., Catlin, G., Lobell, M., Palan, S. *et al.* (2001). Antibiotic activity and characterization of BB-3497, a novel peptide deformylase inhibitor. *Antimicrob. Agents Chemother.* **45**, 563–570.
38. Giglione, C. & Meinnel, T. (2001). Resistance to anti-peptide deformylase drugs. *Expt. Opin. Therap. Targets*, **5**, 415–418.
39. Chen, D. (2000). *In vivo* evaluation of VRC3375, a potent peptide deformylase inhibitor. In *Interscience Conference on Antimicrobial Agents and Chemotherapy—40th Meeting (Part VII), Toronto, Canada, 17–20 September 2000, (Meeting News) Investigational Drugs Daily Highlights, 27th September 2000*, Abstract no. 2175.
40. Wise, R., Andrews, J. M. & Ashby, J. (2002). *In vitro* activities of peptide deformylase inhibitors against Gram-positive pathogens. *Antimicrob. Agents Chemother.* **46**, 1117–1118.
41. Schechter, I. & Berger, A. (1967). On the size of the active site in proteases. I. Papain. *Bochem. Biophys. Res. Commun.* **27**, 157–162.
42. Bradford, M. M. (1976). A rapid and sensitive method for the quantitation of microgram quantities of protein utilizing the principle of protein-dye binding. *Anal. Biochem.* **72**, 248–254.
43. Otwinowski, Z. & Minor, W. (1997). Processing of X-ray diffraction data collected in oscillation mode. *Methods Enzymol.* **276**, 307–332.
44. Collaborative Computational Project Number 4 (1994). The CCP4 suite: programs for protein crystallography. *Acta Crystallog. sect. D*, **50**, 760–763.
45. de La Fortelle, E. & Bricogne, G. (1997). Maximum-likelihood heavy-atom parameter refinement for multiple isomorphous replacement and multiwavelength anomalous diffraction methods. *Methods Enzymol.* **276**, 472–494.
46. Jones, T. A., Zou, J. Y., Cowan, S. W. & Kjeldgaard, M. (1991). Improved methods for binding protein models in electron density maps and the location of errors in these models. *Acta Crystallog. sect. A*, **47**, 110–119.
47. Brünger, A. T. (1992). *X-PLOR Version 3.1. A System for X-ray Crystallography and NMR*, Yale University Press, New Haven, CT.
48. Giglione, C. & Meinnel, T. (2001). Peptide deformylase as an emerging target for antiparasitic agents. *Emerg. Therap. Targets*, **5**, 41–57.
49. Jeanmougin, F., Thompson, J. D., Gouy, M., Higgins, D. G. & Gibson, T. J. (1998). Multiple sequence alignment with Clustal X. *Trends Biochem. Sci.* **23**, 403–405.
50. Page, R. D. M. (1996). TREEVIEW: An application to display phylogenetic trees on personal computers. *Comput. Appl. Biosci.* **12**, 357–358.
51. Hutchinson, E. G. & Thornton, J. M. (1996). PROMOTIF: a program to identify and analyse structural motifs in proteins. *Protein Sci.* **5**, 212–220.

***Edited by R. Huber***

*(Received 26 November 2001; received in revised form 21 May 2002; accepted 27 May 2002)*